



# 7X multiplexed, optofluidic detection of nucleic acids for antibiotic-resistance bacterial screening

G. G. MEENA,<sup>1</sup>  T. A. WALL,<sup>2</sup> M. A. STOTT,<sup>2</sup> O. BROWN,<sup>3</sup> R. ROBISON,<sup>3</sup> A. R. HAWKINS,<sup>2</sup> AND H. SCHMIDT<sup>1,\*</sup>

<sup>1</sup>*School of Engineering, University of California, Santa Cruz, 1156 High Street, Santa Cruz, California 95064, USA*

<sup>2</sup>*Electrical and Computer Engineering Department, Brigham Young University, Provo, Utah 84602, USA*

<sup>3</sup>*Department of Microbiology and Molecular Biology, Brigham Young University, Provo, Utah 84602, USA*  
*\*hshmidt@soe.ucsc.edu*

**Abstract:** Rapid and accurate diagnosis of bacterial infections resistant to multiple antibiotics requires development of new bio-sensors for differentiated detection of multiple targets. This work demonstrates 7x multiplexed detection for antibiotic-resistance bacterial screening on an optofluidic platform. We utilize spectrally multiplexed multi-spot excitation for simultaneous detection of nucleic acid strands corresponding to bacterial targets and resistance genes. This is enabled by multi-mode interference (MMI) waveguides integrated in an optofluidic device. We employ a combinatorial three-color labeling scheme for the nucleic acid assays to scale up their multiplexing capability to seven different nucleic acids, representing three species and four resistance genes.

© 2020 Optical Society of America under the terms of the [OSA Open Access Publishing Agreement](#)

## 1. Introduction

Multiplexed detection is one of the most important capabilities that has to be addressed while developing a new diagnostic system [1]. This arises due to the emergence of multiple pathogens, having comparable biological traits and causing diseases with very similar symptoms [2,3], but responding differently to medical treatments. It is very critical to accurately determine the species and drug susceptibility of the pathogen which is causing a disease to aid the clinician in prescribing the most effective drug for the patient. Several viral disease outbreaks in the last two decades illustrate this need [4–6]. In the case of bacterial infections, antibiotic-resistant bacteria are some of the prime targets that require multiplexed diagnostic platforms [7]. They have become a global health concern due to the inability of current systems to detect them at low concentrations during early stages, and because bacteria can quickly transfer antibiotic-resistance genes among themselves [8].

Several techniques have been developed over the last few years in the field of biotechnology for multiplexed detection of pathogens [9]. These include broad-spectrum methods of parallel detection like multiplex RT-PCR assays [10], surface-functionalization based microarrays [11,12] or combinatorial labeling probes such as nano-strings [13] and nanobarcodes [14] which are all techniques that use various target labeling methods. All of these are reliable techniques that can be employed for the study of genomic and proteomic targets but require a lot of hands-on sample preparation and expensive laboratory techniques. These multiplexed screening methods have been integrated with point-of-care lab-on-a-chip devices aimed at making them accessible, and to reduce the dependence on trained users for complex off-chip assay preparations [15]. A few examples are paper-based setups which use capillary flow-based target separation and surface functionalization [16,17], 3-D microfluidic channels with T and Y junction sample splitters integrated with flexible membrane based micro pumps for reagent mixing [18], and lab-on-a-disk

devices which use centrifugal force for target separation and different spin speeds for reagent mixing [19]. Most of these devices use top down optical image-analysis based detection schemes, the sensitivity and distinguishability of which drops considerably when the number of targets is increased.

More recently, optofluidic devices, which integrate optical waveguides with microfluidics to increase the level of system integration, have emerged as a promising bio-sensor platform [20–22]. In this work, we use a silicon-based bio-photonic sensor platform which uses micron scale anti-resonant-reflecting-optical-waveguides (ARROW) [23]. These devices use a combination of liquid-core and solid-core waveguide for exciting fluorescently tagged targets and for collecting their signals. The sensitive waveguide system with femtoliter excitation volumes has been used for detection of viral pathogens with sensitivity down to single nucleic acids and an analytic limit of detection in the attomolar range [24–26]. They have been integrated with a polydimethylsiloxane (PDMS) based on-chip sample preparation system to demonstrate a complete sample to answer detection platform [27]. Multiplexing capability has been incorporated on this platform via multi-spot excitation patterns generated by multi-mode interference (MMI) waveguides [28]. This concept has been used for spectral [29], spatial [30], and velocity-dependent [31] discrimination between individual fluorescent targets.

In this work we demonstrate the full spectral multiplexing power of MMI waveguides for distinguishing  $2^{M-1}$  targets with  $M$  excitation wavelengths. Specifically, combinatorial labeling with three colors is used for detection of nucleic acids representing seven antibiotic resistant bacterial targets (three bacterial species: *E. coli*, *E. aerogenes*, and *K. pneumoniae*, and four antibiotic resistance genes: VIM, NDM, KPC and IMP) in a single channel).

## 2. Principle and methods

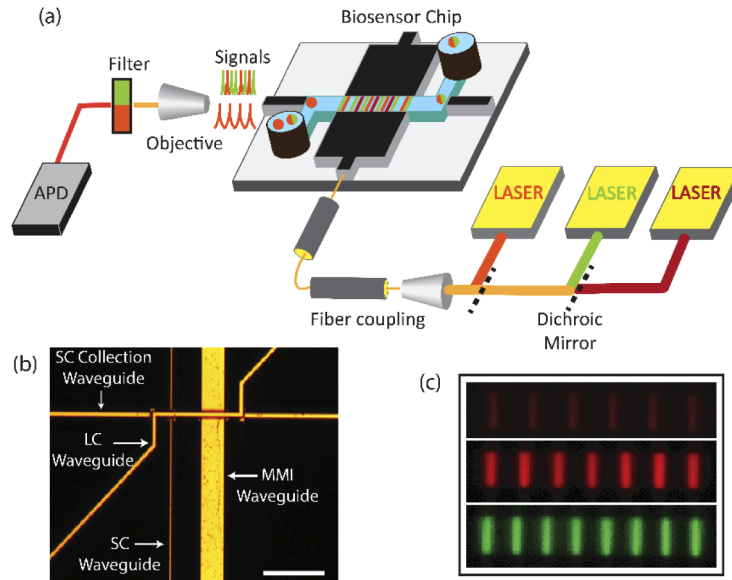
### 2.1. Device and experimental setup design

Figure 1(a) shows a schematic of the ARROW based optofluidic platform. The chip has a solid-core (SC) waveguide orthogonally intersecting a liquid-core (LC) waveguide (See Supplement 1: Device fabrication, Fig. S1) [32–34]. For multiplexing capabilities, the SC waveguide is designed as an MMI waveguide that is wide enough to support multiple modes propagating with different propagation constants. These modes interfere with each other to generate well defined spots at specific distances. MMI waveguides of refractive index  $n$  (here 1.51) are designed to intersect the LC waveguides at a specific distance  $L$ . The width  $W$  (here 75  $\mu\text{m}$ ) and length  $L$  (here 1975  $\mu\text{m}$ ) of the MMI waveguide are chosen so as to generate well defined patterns with  $N_c$  number of spots when excited with light of wavelength  $\lambda_c$  [Eq. (1)]. Figure 1(b) shows the top down optical image of the chip with the SC and MMI waveguides intersecting the LC waveguide.

$$N_c \cdot \lambda_c = \frac{n \cdot W^2}{L}. \quad (1)$$

Here, the MMI waveguides produce six, seven and eight spots in the LC waveguide when excited by 738 nm, 633 nm and 556 nm, respectively. Figure 1(c) shows the pattern generated by the MMI waveguide in the fluorescent dye filled LC waveguide when excited by these three wavelengths. Analytes captured on microbeads are introduced in the LC waveguide through the inlet and moved past the MMI – LC waveguide intersection via pressure driven flow. The MMI waveguide is excited simultaneously by Ti:Sapphire (738 nm), HeNe (633 nm) and solid-state (556 nm) lasers. The fluorescence signals from excited targets which flow past the MMI waveguide are guided along the LC waveguide, captured by the SC collection waveguide (shown in Fig. 1(b)) and detected using an Avalanche Photo Detector (APD) after filtering out excitation lights (Bright Line). The targets excited by the MMI waveguide generate fluorescence signals encoded with distinct temporal pattern based on their specific color combination label. Thus, target information

is fully encoded in the time-domain signal which is demultiplexed using a signal processing algorithm.



**Fig. 1.** (a) Schematic view of experimental setup and optofluidic chip. (b) Top down optical microscope image of a chip (Scale bar: 200μm) (c) Color coded fluorescent dye image of the patterns generated by the MMI waveguide in the LC waveguide.

## 2.2. Nucleic acid assay design and preparation

For target specific capturing and labeling of the nucleic acids, we use a magnetic-bead based sandwich assay. In this study, we choose seven different targets, three of which correspond to bacterial species *E. coli*, *E. aerogenes*, *K. pneumoniae* and the other four corresponding to carbapenem antibiotic resistance genes: *Verona integron metallo-β-lactamase* (VIM), *New Delhi metallo-β-lactamase* (NDM), *Imipenemase* (IMP) and *Klebsiella pneumoniae carbapenemase* (KPC). Because this application involves multiplexed detection of several targets using MMI waveguides, it is not practical to use seven different wavelengths to excite the targets. The number of excitation wavelengths are limited by available fluorescent dye and laser combinations, complexity in the experimental setup design and absorption-emission spectral overlap. This bottleneck can be solved by using a combinatorial color labeling approach which will ensure that signal from each target still has unique spectral information encoded (provided there is no absorption-emission overlap between the different labels). Thus, using  $M$  wavelengths, we can now have multiplexing scaled up to  $2^M - 1$ . In this work, we demonstrate 7X multiplexed target detection of an antibiotic-resistant bacterial panel using three different color labels Dark Red (DR), Red (R) and Green (G) corresponding to wavelengths 738 nm, 633 nm and 556 nm to create seven distinguishable color combinations (DR, R, G, DR-R, R-G, G-DR, DR-R-G).

For the fluorescence assays, 3 μM of synthetic oligomers that represent part of the gene corresponding to the target is mixed and incubated with 10 μM of multiple target specific fluorescent probe oligomers. The types of fluorescent probes correspond to the assigned color combination code for the target (Fig. 2(b)). The hybridized target-probe structure is captured by streptavidin-coated magnetic beads saturated with target-specific biotinylated pulldown oligomers (Fig. 2(a), See Supplement 1: Assay preparation). Each magnetic bead has a maximum of about  $10^5$  binding sites. All unbound targets and beacons are washed off using a magnet and multiple

buffer exchanges. In Supplement 1, Table S1 summarizes the targets, fluorescent probes and capture oligomers used.

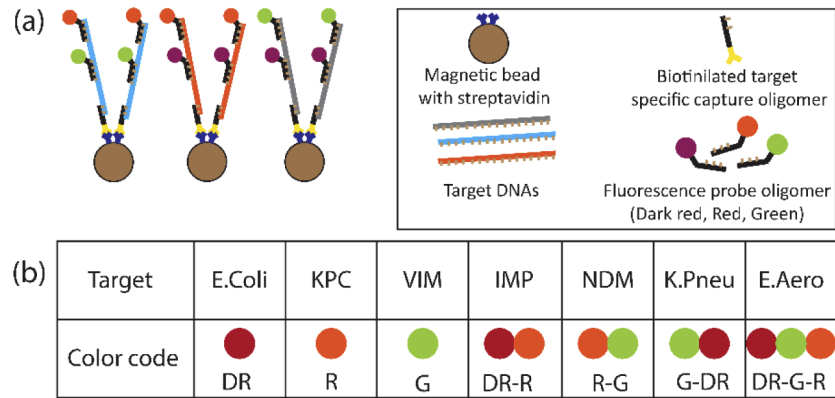


**Fig. 2.** (a) Schematic image of magnetic-bead based assays with targets combinatorially labeled with dark red, red and green colors. (b) Color codes used to label the seven different antibiotic resistance gene/species targets [DR-Dark Red, R-Red, G-Green].

### 3. Results and discussion

#### 3.1. Single color tagged target detection

First, the ability of the device and the signal processing algorithm to accurately detect and identify individual targets is demonstrated. To start with, we introduced beads with single color tagged *E. coli* target labeled with dark red fluorophore in the LC waveguide of the device. The MMI waveguide is thus excited only with 738 nm wavelength. Figure 3(a)(i) shows the fluorescence signals from the *E. coli* targets, and the black dashed line depicts the threshold for detecting a target defined as the highest background level when the channel is excited by all three lasers 8 counts/10 $\mu$ s, but contains no fluorescent targets. Zooming in on an event from a single bead shows a signal with six peaks which corresponds to the excitation pattern generated by the MMI waveguide (Fig. 3(a)(ii)). For automated target identification we assess signal from each individual bead using Eq. (2).

$$S(t, \delta t_C)_C = \left\{ \prod_{i=0}^{N_C-1} F(t - i \cdot \delta t_C) \right\}^{\frac{1}{N_C-1}}. \quad (2)$$

Here,  $F(t)$  is the measured fluorescence signal and  $N_c$  is the number of spots generated by the MMI waveguide for different colors. The product in Eq. (2) represents a “shift-multiply” approach in which  $F(t)$  is shifted repeatedly by the characteristic time spacing  $\delta t_c$  for a given pattern. If a particular spot number is present, this process will result in a large  $S(t)$  value [29,35].  $\delta t_c$  for a particular event is determined by dividing the total duration of each multi-spot signal by the number of spots  $N_C$  for each pattern (See Supplement 1:  $\delta t_c$  calculation). By calculating  $S(t)_C$  for each  $N_c$ , a map is generated showing which color channels dominate above set thresholds, thus indicating the corresponding color code tag and uniquely identifying the target captured on the bead. Figure 3(a)(iii) shows the map of a correctly identified *E. coli* signal of Fig. 3(a)(ii), dominating only on the dark red channel.  $S(t)_C$  values of all the detected *E. coli*-carrying beads are plotted as histograms in Fig. 4(a). The dotted vertical line indicates the threshold set for each channel defined as the average  $S(t)_C$  value plus one standard deviation of signals from individual experiments of all seven targets. A correctly identified *E. coli* signal will only have  $S(t)_{DR}$  above

the threshold. 91.6% of all the analyzed *E. coli* events had  $S(t)_{DR}$  above threshold and  $S(t)_R$  &  $S(t)_G$  below threshold (the black colored symbols in Fig. 3(a)(i) mark the incorrectly identified fluorescence signals). The same control experiments were also done for the other two single color tagged targets (KPC and VIM), which were detected with an average accuracy of 90%

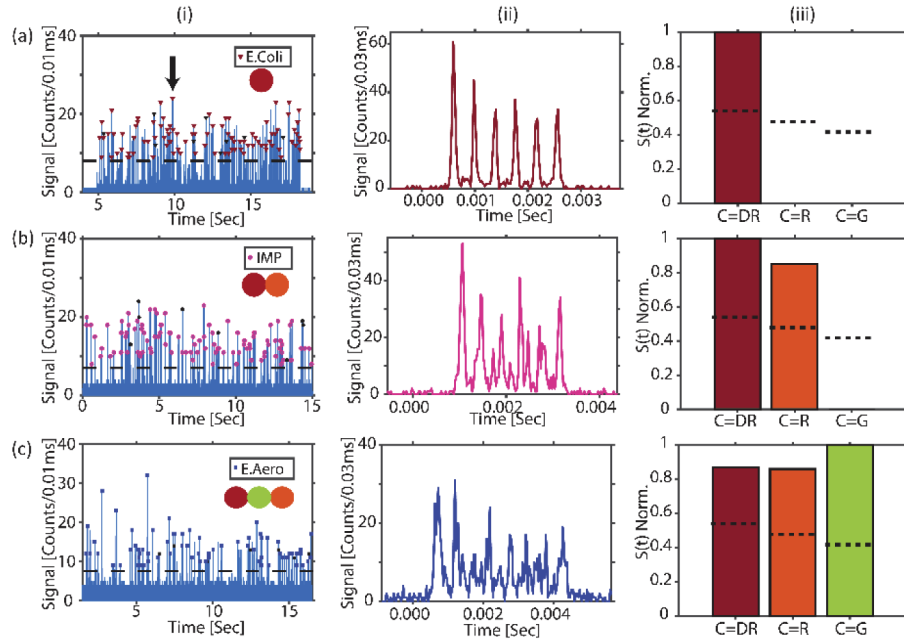


**Fig. 3.** Single-target experiments. (a) *E. coli* detection: (i) Detected fluorescence signals when beads with *E. coli* targets are flowed through the chip and excited by the MMI waveguide; colored (black) symbols on each event represent correctly (incorrectly) identified targets. The dashed line indicates the threshold for particle detection. (ii) Zoomed-in signal from a single bead. (iii) Bar histogram map of  $S(t)_C$  of a correctly identified *E. coli* signal. (b) and (c) same analysis for IMP and *E. aerogenes* targets.

### 3.2. Multi color target detection

Figure 3(b)(i) and Fig. 3(c)(i) show fluorescence signals from two separate experiments to test individual multi-color labeled targets. In the first case, the chip has beads with IMP target labeled with two colors (DR-R) flowing in the LC waveguide with MMI waveguides excited simultaneously by 738 nm and 633 nm lasers. Signals in Fig. 3(c)(i) represent the case of *E. aerogenes* targets labeled with three colors (DR-R-G) in the chip excited with all three corresponding lasers. While signals from single color tagged targets could also be identified by simply counting the number of peaks, events from multicolor tagged targets are superpositions of the multi-peak-signals corresponding to the color codes of the target (Fig. 3(b)(ii) and Fig. 3(c)(ii)). On these mixed signals, Eq. (2) must be applied and  $S(t)_C$  maps for individual events are generated. The maps show that the signal from the beads with IMP target is dominant in both dark red and red color channels whereas the signals of beads with *E. aerogenes* target shows up in dark red, red and green color channels, thus enabling a correct identification (Fig. 3(b)(iii) and Fig. 3(c)(iii)). From the analysis of all the detected IMP-carrying beads and *E. aerogenes*-carrying beads (Fig. 4(b) and Fig. 4(c)), an average of 90.2% of the events were correctly identified. This demonstrates successful detection of both two-color labeled and triple-color labeled targets with very similar accuracies using this scheme. Similar experiments were also done with the other

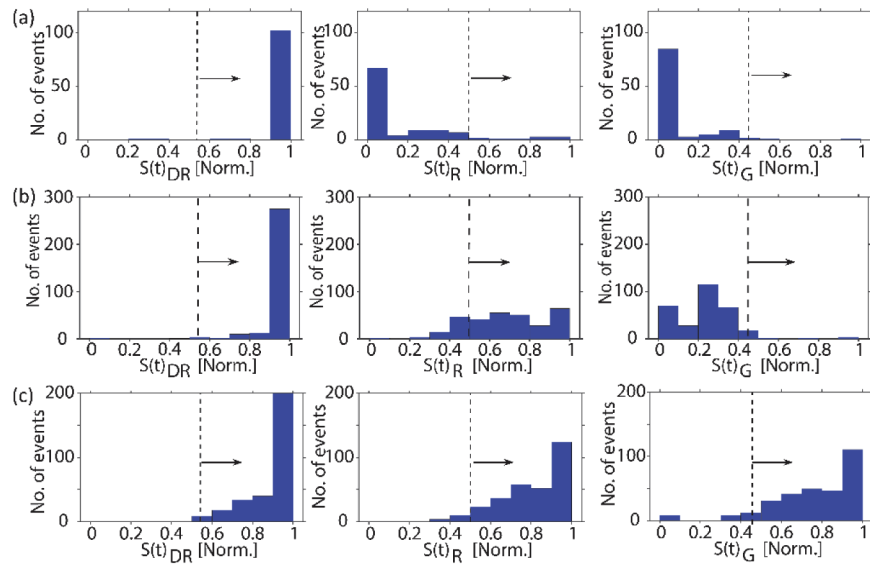


**Fig. 4.** (a) Histogram of  $S(t)_C$  values of all the detected single colored (DR) *E. coli*-carrying beads. Most of the signals dominate only in the dark red channel ((b) and (c) are from two-color (DR-R) IMP targets and three-color (DR-R-G) *E. aerogenes* targets).

multi-color tagged targets NDM and *K. pneumoniae*. Targets were detected at an average rate of 5.6 events/sec with an SNR of 39 (background noise of 0.39 counts/10 $\mu$ s) and 85% accuracy, demonstrating the ability of the chip to rapidly detect targets with good sensitivity.

### 3.3. 7X multiplexed detection

For the full multiplexed assay, equal concentrations of all seven targets were mixed and flowed through the chip. The MMI waveguide is now simultaneously excited with 738 nm, 633 nm and 556 nm lasers. The signals from all seven targets collected by the APD are demultiplexed by processing each signal using Eq. (2) and generating the  $S(t)_C$  map. Based on which colors dominate in the map, the spectral information in the signal is decoded and thus, the target it corresponds to is identified.

Figure 5 shows the fluorescence signal trace with all seven targets simultaneously detected. We detect an average of  $(1.8 \pm 0.7) \times 10^6$  beads/mL per target, which is about 69% of the expected concentration. While preparing the beads with fluorescent tagged targets, an incremental ratio of 1:10:30 (bead: target: fluorescent-probe) was used to saturate each element of the bead. However, only a fraction of the binding sites of the magnetic bead is hybridized with the target-fluorescent probe complex due to inaccuracies in concentration and steric hindrance between targets captured on the bead. The accuracy of the signal processing algorithm depends on the quality and strength of the signal. To ensure maximum precision of the signal processing algorithm, a very conservative threshold (8counts/10 $\mu$ s) was used to pick only signals above the highest background photon count. Thus, some signals with lower signal strength are visible below this threshold, but are not counted (See Supplement 1: Fig. S3). This accounts for the difference in detected and expected concentration of the beads in the above experiment. In the future, other signal decomposition techniques such as wavelet transformation [36,37] can be used to extract low intensity signals close to the background level.

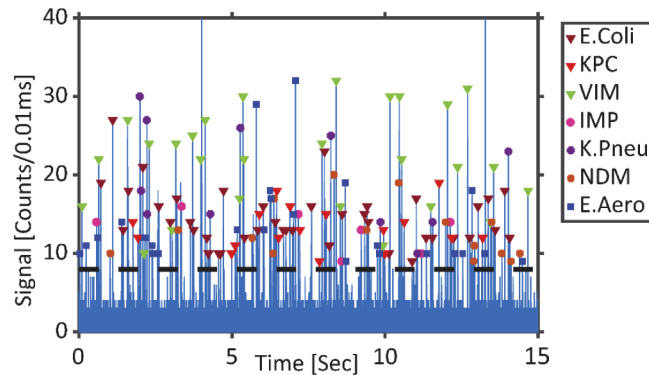


**Fig. 5.** Fluorescence signals from all seven bacterial targets are flowed simultaneously through the chip, excited by all three lasers and identified; dashed line: threshold for target detection.

#### 4. Conclusion

In this work, we have demonstrated 7X multiplexed detection of three bacterial species and four resistance genes on an optofluidic chip by combinatorial labeling of targets using three colors. A time domain signal processing algorithm was used to demultiplex the signals detected by the chip. This technology can be further extended to the detection of single nucleic acid targets at clinically relevant concentrations by the target-specific tagging of individual DNAs with multiple fluorophores [24] or brighter probes [25]. Multiplexing capability of the device can be scaled up to higher orders by introducing multiple LC waveguide channels in a single chip [30] and also via multi-channel velocity multiplexing [31].

#### Funding

W. M. Keck Center for Nanoscale Optofluidics, University of California, Santa Cruz; National Institutes of Health (1R01AI116989-01, 4R33AI100229).

#### Disclosures

A.R.H and H.S have financial interest in Fluxus Inc. which is developing optofluidic devices.

See [Supplement 1](#) for supporting content.

#### References

1. N. M. Cirino, K. A. Musser, and C. Egan, "Multiplex diagnostic platforms for detection of biothreat agents," *Expert Rev. Mol. Diagn.* **4**(6), 841–857 (2004).
2. S. Suwanmanee and N. Luplertlop, "Dengue and Zika viruses: lessons learned from the similarities between these Aedes mosquito-vectorized arboviruses," *J. Microbiol.* **55**(2), 81–89 (2017).
3. L. D. Raesa, C. S. Kraft, G. G. Olinger, and L. E. Hensley, "Viral Hemorrhagic Fever Diagnostics," *Clin. Infect. Dis.* **62**(2), 214–219 (2015).
4. D. Musso, V. Mai Cao-Lormeau, and D. J. Gubler, "Zika virus: following the path of dengue and chikungunya?" *Lancet* **386**(9990), 243–244 (2015).
5. V. Colizza, A. Barrat, M. Barthélemy, and A. Vespignani, "Predictability and epidemic pathways in global outbreaks of infectious diseases: the SARS case study," *BMC Med.* **5**(1), 34 (2007).
6. A. R. Sahin, A. Erdogan, P. M. Agaoglu, Y. Dineri, A. Y. Cakirci, M. E. Senel, R. A. Okyay, and A. M. Tasdogan, "2019 Novel Coronavirus (COVID-19) Outbreak: A Review of the Current Literature," *EJMO* **4**(1), 1–7 (2020).
7. R. Laxminarayan, A. Duse, C. Wattal, A. K. M. Zaidi, H. F. L. Wertheim, N. Sumpradit, E. Vlieghe, G. L. Hara, I. M. Gould, H. Goossens, C. Greko, A. D. So, M. Bigdeli, G. Tomson, W. Woodhouse, E. Ombaka, A. Q. Peralta,

- F. N. Qamar, F. Mir, S. Kariuki, Z. A. Bhutta, A. Coates, R. Bergstrom, G. D. Wright, E. D. Brown, and O. Cars, "Antibiotic resistance—the need for global solutions," *Lancet Infect. Dis.* **13**(12), 1057–1098 (2013).
8. U.S Centers for Disease Control, Antibiotic Resistance Threats in the United States, (CDC, 2019).
  9. V. Pallás, D. James, and J. A. Sánchez-Navarro, "Recent Advances on the Multiplex Molecular Detection of Plant Viruses and Viroids," *Front. Microbiol.* **9**, 2087 (2018).
  10. S. B. Pujol, A. Vabret, L. Legrand, J. Dina, S. Gouarin, J. P. Lecherbonnier, B. Pozzetto, C. Ginevra, and F. Freymuth, "Development of three multiplex RT-PCR assays for the detection of 12 respiratory RNA viruses," *J. Virol. Methods* **126**(1-2), 53–63 (2005).
  11. T. W. Chang, "Binding of cells to matrixes of distinct antibodies coated on solid surface," *J. Virol. Methods* **65**(1-2), 217–223 (1983).
  12. R. Becher, F. Weihmann, H. B. Deising, and S. Gr Wirsal, "Development of a Novel Multiplex DNA Microarray for Fusarium Graminearum and Analysis of Azole Fungicide Responses," *BMC Genomics* **12**(1), 52 (2011).
  13. G. K. Geiss, R. E. Bumgarner, B. Birditt, T. Dahl, N. Dowidar, D. L. Dunaway, H. P. Fell, S. Ferree, R. D. George, T. Grogan, J. J. James, M. Maysuria, J. D. Mitton, P. Oliveri, J. L. Osborn, T. Peng, A. L. Ratcliffe, P. J. Webster, E. H. Davidson, L. Hood, and K. Dimitrov, "Direct multiplexed measurement of gene expression with color-coded probe pairs," *Nat. Biotechnol.* **26**(3), 317–325 (2008).
  14. Y. Li, Y. Thi, H. Cu, and D. Luo, "Multiplexed detection of pathogen DNA with DNA-based fluorescence nanobarcodes," *Nat. Biotechnol.* **23**(7), 885–889 (2005).
  15. C. Dincer, R. Bruch, A. Kling, P. S. Dittrich, and G. A. Urban, "Multiplexed Point-of-Care Testing – xPOCT," *Trends Biotechnol.* **35**(8), 728–742 (2017).
  16. N. R. Pollock, J. P. Rolland, S. Kumar, P. D. Beattie, S. Jain, F. Noubary, V. L. Wong, R. A. Pohlmann, U. S. Ryan, and G. M. Whitesides, "A paper-based multiplexed transaminase test for low-cost, point-of-care liver function testing," *J. Microbiol.* **4**(152), 152ra129 (2012).
  17. S. Ahmed, M. P. N. Bui, and A. Abbas, "Paper-based chemical and biological sensors: Engineering aspects," *Biosens. Bioelectron.* **77**, 249–263 (2016).
  18. C. D. Chin, T. Laksanasopin, Y. Kee Cheung, D. Steinmiller, V. Linder, H. Parsa, J. Wang, H. Moore, R. Rouse, G. Umvilighozo, E. Karita, L. Mwambarangwe, S. L. Braunstein, J. van de Wijkert, R. Sahabo, J. E. Justman, W. El-Sadr, and S. K. Sia, "Microfluidics-based diagnostics of infectious diseases in the developing world," *Nat. Med.* **17**(8), 1015–1019 (2011).
  19. R. Burger, L. Amato, and A. Boisen, "Detection methods for centrifugal microfluidic platforms," *Biosens. Bioelectron.* **76**, 54–67 (2016).
  20. V. Lien, Y. Berdichevsky, and Y. H. Lo, "A prealigned process of integrating optical waveguides with microfluidic devices," *IEEE Photonics Technol. Lett.* **16**(6), 1525–1527 (2004).
  21. X. Fan and I. M. White, "Optofluidic microsystems for chemical and biological analysis," *Nat. Photonics* **5**(10), 591–597 (2011).
  22. H. Schmidt and A. R. Hawkins, "The photonic integration of non-solid media using optofluidics," *Nat. Photonics* **5**(10), 598–604 (2011).
  23. H. Schmidt and A. R. Hawkins, "Optofluidic waveguides: I. Concepts and implementations," *Microfluid. Nanofluid.* **4**(1-2), 3–16 (2008).
  24. H. Cai, J. W. Parks, T. A. Wall, M. A. Stott, A. Stambaugh, K. Alfson, A. Griffiths, R. A. Mathies, R. Carrion, J. L. Patterson, A. R. Hawkins, and H. Schmidt, "Optofluidic analysis system for amplification-free, direct detection of Ebola infection," *Sci. Rep.* **5**(1), 14494 (2015).
  25. K. Du, M. Park, A. Griffiths, R. Carrion, J. Patterson, H. Schmidt, and R. Mathies, "Microfluidic System for Detection of Viral RNA in Blood Using a Barcode Fluorescence Reporter and a Photocleavable Capture Probe," *Anal. Chem.* **89**(22), 12433–12440 (2017).
  26. K. Du, H. Cai, M. Park, T. A. Wall, M. A. Stott, K. J. Alfson, A. Griffiths, R. Carrion, J. L. Patterson, A. R. Hawkins, H. Schmidt, and R. A. Mathies, "Multiplexed efficient on-chip sample preparation and sensitive amplification-free detection of Ebola virus," *Biosens. Bioelectron.* **91**, 489–496 (2017).
  27. J. W. Parks, M. A. Olson, J. Kim, D. Ozcelik, H. Cai, R. Carrion, J. L. Patterson, R. A. Mathies, A. R. Hawkins, and H. Schmidt, "Integration of programmable microfluidics and on-chip fluorescence detection for biosensing applications," *Biomicrofluidics* **8**(5), 054111 (2014).
  28. L. B. Soldano and E. C. M. Pennings, "Optical Multi-Mode Interference Devices Based on Self-Imaging: Principles and Applications," *J. Light. Technol.* **13**(4), 615–627 (1995).
  29. D. Ozcelik, J. W. Parks, T. A. Wall, M. A. Stott, H. Cai, J. W. Parks, A. R. Hawkins, and H. Schmidt, "Optofluidic wavelength division multiplexing for single-virus detection," *Proc. Natl. Acad. Sci. U. S. A.* **112**(42), 12933–12937 (2015).
  30. D. Ozcelik, A. Jain, A. Stambaugh, M. A. Stott, J. W. Parks, A. Hawkins, and H. Schmidt, "Scalable Spatial-Spectral Multiplexing of Single-Virus Detection Using Multimode Interference Waveguides," *Sci. Rep.* **7**(1), 12199 (2017).
  31. J. A. Black, V. Ganjalizadeh, J. W. Parks, and H. Schmidt, "Multi-channel velocity multiplexing of single virus detection on an optofluidic chip," *Opt. Lett.* **43**(18), 4425–4428 (2018).
  32. T. Wall, J. McMurray, G. G. Meena, V. Ganjalizadeh, H. Schmidt, and A. R. Hawkins, "micromachines Optofluidic Lab-on-a-Chip Fluorescence Sensor Using Integrated Buried ARROW (bARROW) Waveguides," *Micromachines* **8**(8), 252 (2017).



33. M. A. Stott, V. Ganjalizadeh, G. G. Meena, J. McMurray, M. Olsen, M. Orfila, H. Schmidt, and A. R. Hawkins, "Buried Rib SiO<sub>2</sub> Multimode Interference Waveguides for Optofluidic Multiplexing," *IEEE Photonics Technol. Lett.* **30**(16), 1487–1490 (2018).
34. M. A. Stott, V. Ganjalizadeh, M. H. Olsen, M. Orfila, J. McMurray, H. Schmidt, and A. R. Hawkins, "Optimized ARROW-Based MMI Waveguides for High Fidelity Excitation Patterns for Optofluidic Multiplexing," *IEEE J. Quantum Electron.* **54**(3), 1–7 (2018).
35. D. Ozcelik, M. A. Stott, J. W. Parks, J. A. Black, T. A. Wall, A. R. Hawkins, and H. Schmidt, "Signal-to-noise enhancement in optical detection of single viruses with multispot excitation," *IEEE J. Sel. Top. Quantum Electron.* **22**(4), 6–11 (2016).
36. Y. Zheng, R. Fan, C. Qiu, Z. Liu, and D. Tian, "An improved algorithm for peak detection in mass spectra based on continuous wavelet transform," *Int. J. Mass Spectrom.* **409**, 53–58 (2016).
37. P. Du, W. A. Kibbe, and S. M. Lin, "Improved peak detection in mass spectrum by incorporating continuous wavelet transform-based pattern matching," *Bioinformatics* **22**(17), 2059–2065 (2006).